Effects of Step Pool Porosity upon Flow Aeration and Energy Dissipation on Pooled Stepped Spillways

Stefan Felder[1] and Hubert Chanson[2]

Abstract: The hydraulics of stepped spillways with flat steps has been studied for the last three decades, including for embankment dam slopes, but studies of alternative stepped designs are limited. In this study, a pooled stepped spillway was investigated in a relatively large-size facility, and three different pool wall porosities were tested. The flow patterns, the macro- and microscopic air-water flow properties, and the energy dissipation performances were recorded; the results were compared with the flat stepped spillway design for the same chute slope ($\theta = 26.6°$). The investigations highlighted a close agreement between air-water flow properties on the configurations in terms of void fraction, turbulence levels, bubble count rate, and chord sizes. The interfacial velocity distributions showed larger interfacial velocity on the pooled step configurations of approximately 5–10% linked with a reduced flow depth. On the porous pooled stepped spillways, the interfacial velocities within the cavity highlighted the flow through the pores and the reduction in cavity recirculation. The porous pooled weir reduced the form drag, and the residual energy was approximately 1.5–2 times larger on the porous pooled stepped chute with $Po = 31\%$ and approximately 1.3 times larger on the porous steps with $Po = 5\%$ compared with the flat stepped chute. The flat step design appeared to be the most advantageous in terms of flow stability and energy dissipation performance. **DOI: 10.1061/(ASCE)HY.1943-7900.0000858.**

Author keywords: Porous pooled steps; Pooled steps; Stepped spillway; Flow aeration; Energy dissipation; Flow resistance.

Introduction

Stepped spillways are designed for both gravity dams and embankment structures (Chanson 2001). The steps act as large rough elements, thus increasing the air entrainment and energy dissipation performances compared with smooth chutes (Rajaratnam 1990; Chanson 1994; Chamani and Rajaratnam 1999). The stepped design is compatible with a number of modern construction techniques, including roller compacted concrete (RCC). The steps increase the flow aeration, thus reducing the cavitation risk.

Stepped spillways are typically designed for large flow rates in the skimming flow regime. Detailed air-water flow experiments have been performed on flat uniform steps with embankment dam slopes and the aeration and energy dissipation performances are well documented (e.g., Ohtsu et al. 2004; Gonzalez and Chanson 2007; Felder and Chanson 2009a; Bung 2011).

However, the stepped spillway design may be applied to nonuniform steps (e.g., Tillot Dam, France) (Chanson 2001), downward inclined steps (e.g., Brushes Clough Dam, U.K.) (Baker 1994), changing channel slope (e.g., New Victoria Dam, Australia) (Felder 2013), pooled steps (e.g., Sorpe Dam, Germany) (Thorwarth 2008), and some hydraulic structures were designed with gabion steps (e.g., Gabion Dam structure, West Cornfield, New Mexico). More complex stepped spillway designs were also considered, i.e., triangular vanes across the step cavities (Gonzalez and Chanson 2008), stepped chutes with wedge-shaped concrete blocks (Relvas and Pinheiro 2008), nonuniform stepped spillways (Felder and Chanson 2011), and over gabion stepped weirs (Peyras et al. 1992). The air-water flows on pooled stepped spillways were investigated with channel slopes of $\theta = 14.6°$, 18.6°, and 30° (André 2004; Kökpinar 2004; Thorwarth 2008). Thorwarth (2008) and Felder (2013) researched self-induced instabilities on a pooled stepped spillway with $\theta = 8.9°$, which might cause a risk for safety as documented for the Sorpe Dam (Chanson 2001; Thorwarth 2008). On the same spillway facility ($\theta = 8.9°$), Felder and Chanson (2013b) compared the aeration and energy dissipation performances on stepped configurations with flat, pooled, and combination of flat and pooled steps. A comparative analysis of air entrainment, instabilities, and energy dissipation on flat and pooled stepped spillways with $\theta = 8.9°$ and $\theta = 26.6°$ was performed by Felder and Chanson (2013a). Recently, Guenther et al. (2013) studied the air-water flow patterns and energy dissipation performances on stepped spillways with in-line and staggered configurations of flat and pooled steps with $\theta = 26.6°$.

In this study, further pooled step designs were investigated for a chute slope $\theta = 26.6°$ (2 H:1 V). Three pool wall porosities were tested: $Po = 0$, 5, and 31%. A porosity of 31% was approximately the porosity of gabion pool walls, and the porosity $Po = 5\%$ was tested to reflect a low water discharge drainage system for pooled stepped spillways. The present study focused upon the flow patterns, the aeration, and the energy dissipation performances on the porous pooled stepped chutes; the results were compared with the pooled step design ($Po = 0$) and the flat reference configuration.

Experimental Facility, Instrumentation, and Flow Conditions

The experimental study was conducted in a large-size stepped spillway facility with a 7-m-long, 0.52-m-wide test section with a slope of 26.6° and perspex sidewalls for flow visualization. The channel consisted of 10 plywood steps with step height $h = 10$ cm.

[1]Postdoctoral Researcher, School of Civil Engineering, Univ. of Queensland, Brisbane QLD 4072, Australia (corresponding author). E-mail: stefan.felder@uqconnect.edu.au

[2]Professor, School of Civil Engineering, Univ. of Queensland, Brisbane QLD 4072, Australia. E-mail: h.chanson@uq.edu.au

Note. This manuscript was submitted on December 9, 2012; approved on December 6, 2013; published online on January 17, 2014. Discussion period open until June 17, 2014; separate discussions must be submitted for individual papers. This paper is part of the ***Journal of Hydraulic Engineering***, © ASCE, ISSN 0733-9429/04014002(11)/$25.00.

The pooled step weirs were 3.1 cm high and 1.5 cm thick [Fig. 1(a)]. The experiments encompassed four stepped spillway configurations—flat steps, pooled steps ($Po = 0$), and porous pooled steps with $Po = 5\%$ and $Po = 31\%$ (Fig. 1). The pores of the porous pooled steps were 5-mm-diameter holes drilled into the pooled weirs with a thickness of 1.5 cm. The porous configuration with $Po = 31\%$ has 254 holes distributed evenly over four lines, whereas the configuration with $Po = 5\%$ consists of 41 holes distributed over two rows in the upper and lower section of the weir [Figs. 1(b and c)]. The porous pooled configurations were limited to one pore size, two pore distributions, and one pool weir height, and scale effects could exist based upon the porous configurations.

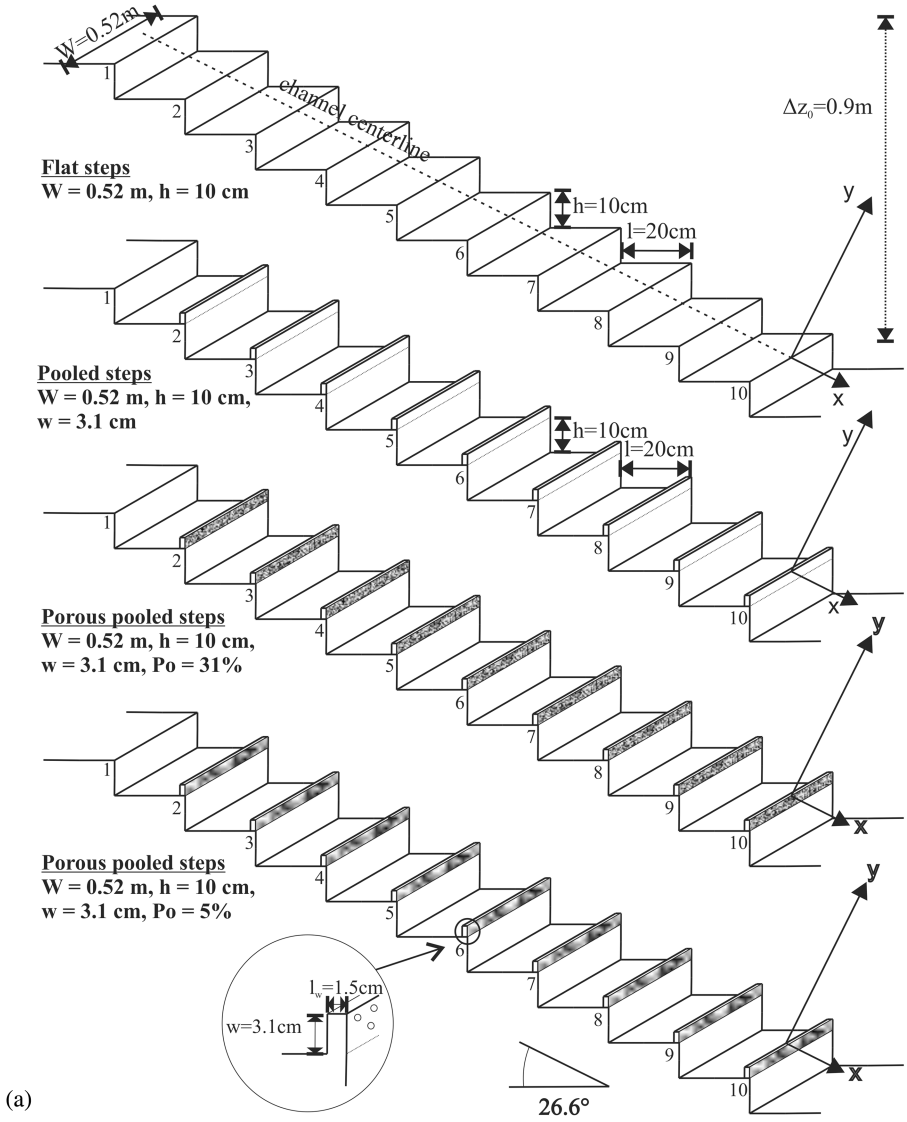

(a)

(b)

(c)

Fig. 1. Stepped spillway configurations with flat, pooled, and porous pooled steps ($\theta = 26.6°$): (a) definition of step numbering and first measurement position on flat and pooled steps ($y = 0$); (b) porous pooled steps: $Po = 31\%$, looking downstream; (c) porous pooled steps: $Po = 5\%$, looking downstream

For all experiments, the equilibrium flow conditions were not achieved owing to the length of the stepped chute.

Constant flow rates were supplied by a large upstream intake basin that supplied smooth, waveless inflows into the test section through a long sidewall convergent with a 4.23:1 contraction ratio. At the upstream end of the test section, the flow was controlled by a broad-crested weir with height of 1 m, width $W = 0.52$ m, length of 1.01 m, and an upstream rounded corner of 0.08 m. The discharge was calibrated with detailed velocity and pressure measurements with a Prandtl-pitot tube (Felder and Chanson 2012)

$$q_w = \left(0.92 + 0.153 \times \frac{H_1}{W}\right) \times \sqrt{g \times \left(\frac{2}{3} \times H_1\right)^3} \quad (1)$$

where q_w = water discharge per unit width; H_1 = upstream total head; and g = gravity acceleration constant.

For all experimental configurations, detailed visual observations of the flow patterns were conducted using a Canon EOS450D dSLR and a Canon Digital IXUS55 camera (Table 1). Table 1 lists the experimental flow conditions for all step configurations comprising flow rates between $0.003\ \text{m}^2/\text{s} < q_w < 0.282\ \text{m}^2/\text{s}$ including nappe, transition, and skimming flows. The experiments were conducted based upon a Froude similitude, and the dimensionless discharge was expressed as d_c/h with d_c the critical flow depth. The air-water flow measurements were conducted with a double-tip conductivity probe (inner diameter $\text{Ø} = 0.25$ mm) in transition and skimming flows for flow rates $0.073\ \text{m}^2/\text{s} < q_w < 0.250\ \text{m}^2/\text{s}$ equaling Reynolds numbers of $2.9 \times 10^5 < R < 9.9 \times 10^5$. Hence, the Reynolds numbers were large enough to avoid significant scale effects as identified in air-water flows on stepped spillways (Boes and Hager 2003; Felder and Chanson 2009b). The leading and trailing tips of the probe were offset in the longitudinal direction by $\Delta x = 7.2$ mm with a transverse separation of $\Delta z = 2.1$ mm. The probe was supported by a trolley system and the positioning of the probe normal to the pseudobottom was performed with a Mitutoyo digital ruler mounted on a fine adjustment screw-drive mechanism. The error in the translation of the probe in the direction normal to the flow was less than 0.5 mm. The accuracy on the longitudinal probe position was estimated as $\Delta x < +/- 0.5$ cm. All measurements were conducted with an electronic system (Reference UQ82.518), and the signal was acquired with a high-speed data acquisition system (NI USB-6251), and self-designed LabVIEW data acquisition software. Based upon a sensitivity analysis, a sampling duration of 45 s, and a sampling rate of 20 kHz per sensor were identified as optimum for the accurate recording of the air-water flow properties. More details about the experimental facility, the data acquisition, and analysis can be found in Felder (2013).

Air-Water Flow Patterns

The air-water flows on the flat stepped spillway exhibited typical flow patterns in the nappe, transition, and skimming flow regimes with increasing discharge. For the smaller flow rates in the nappe flow regime, the water was cascading down the steps in free-falling nappes as previously observed in stepped spillway flows (Toombes 2002). For intermediate discharges in the transition flow regime, small instabilities were observed, including strong droplet splashing and flapping mechanism within the air pockets of the step cavities. In the skimming flow regime, the water looked smooth and glassy at the upstream end, whereas an air-water flow existed with surface parallel to the pseudobottom formed by the step edges downstream of the inception point of air entrainment (e.g., Rajaratnam 1990).

On the pooled stepped spillway, the air-water flow patterns were comparable to the flat steps, exhibiting three flow regimes depending upon the flow rate. The changes in flow regimes for the flat and pooled step designs were in good agreement and compared well with previous studies on embankment dams with similar channel slope (Felder and Chanson 2009a). For the smallest flow rates $d_c/h < 0.45$, a nappe flow regime was observed, and the water discharged in a succession of free-falling nappes from one step pool to the following. For dimensionless flow rates $0.3 < d_c/h < 0.45$, small instabilities of the free-falling nappes were observed. The instabilities resulted from a pulsating flow within the first step cavity, which caused small deviations of the free-falling nappes (Fig. 2). These flow disturbances were much smaller compared with the observations of Thorwarth (2008) and Felder (2013) on a pooled stepped spillway with $\theta = 8.9°$. Although the instabilities for the

Table 1. Summary of Experimental Configurations and Flow Conditions for the Stepped Spillways with Flat, Pooled, and Porous Pooled Steps ($\theta = 26.6°$, $h = 0.1$ m)

Configuration	W (m)	Po	q_w (m^2/s)	d_c/h	R
Flat steps	Not applicable	Not applicable	0.008–0.262	0.18–1.91	$3.1 \times 10^4 - 1.0 \times 10^6$
Pooled steps	0.031	0	0.004–0.267	0.11–1.94	$1.5 \times 10^4 - 1.1 \times 10^6$
Porous pooled steps	0.031	5%	0.003–0.282	0.10–2.01	1.3×10^4–1.1×10^6
Porous pooled steps	0.031	31%	0.003–0.234	0.10–1.77	1.3×10^4–9.3×10^5

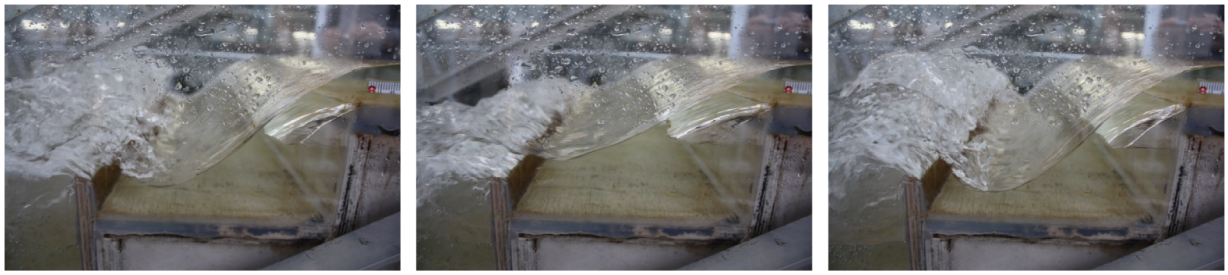

(a) (b) (c)

Fig. 2. Pulsating flows in first step cavity in nappe flow regime on the pooled stepped spillway: $d_c/h = 0.40$, $q_w = 0.025\ \text{m}^2/\text{s}$, $\text{R} = 1.0 \times 10^5$

pooled stepped spillway with $\theta = 26.6°$ were smaller, the pulsating flow in the first step cavity must be taken into consideration by design engineers to allow a safe operation of the pooled stepped structure. For $d_c/h \geq 0.45$, the referred instability was not observed, and the transition and skimming flows were similar to the corresponding flat stepped spillway with stable cavity recirculation movements in skimming flows. The flow depth was larger than on flat stepped chutes because of the pool weir height. Further small upwards directed jets were caused by the pooled weir at the downstream end of each cavity.

The flow patterns on the porous pooled stepped spillways also exhibited typical nappe, transition, and skimming flow regimes. Overall, the observations were in good agreement with the flow patterns on the pooled stepped spillway; although for all flow rates, differences were caused by small discharges through the pores in the porous pooled weirs. An estimation of the discharge through the pores was conducted using resistance coefficients (Idelchik 1994) and the energy equation across the porous pooled wall

$$\Delta H_{(Po)} = \frac{\zeta \times U_{Po}^2}{2 \times g} \tag{2}$$

where $\Delta H_{(Po)}$ = energy difference between the two sides of the porous wall (in this study, the difference in free-surface elevation between one pool weir height upstream and downstream of the pool weir, identified using visual observations); ζ = resistance coefficient for a perforated thick plate (Idelchik 1994); and U_{Po} = streamwise velocity of the discharge through the pores. For skimming flows, the flow discharge through the pores based upon stationary flow considerations was estimated at less than 7% of the total flow discharge for the porous configuration $Po = 31\%$ and less than 1% for $Po = 5\%$. In transition and nappe flows, the discharges through the pores were comparatively larger because the downstream side of the pooled weir was not submerged and a void existed. The porous discharge calculation was a rough estimate, and the recirculations within the cavity, the irregular cavity ejections, and the nonhorizontal angle between flow and pool weir might affect the porous flow.

For the smallest flow rates, a nappe flow regime was observed for both porous pooled configurations. The flow pattern was similar to the nappe flows on the pooled stepped spillway, but some flow appeared through the pores. Importantly, on both porous pooled stepped spillways, no pulsations were observed in the first pooled cavity and no instabilities of the free-falling nappes were present. The pores tended to balance the pressure between adjacent pooled cavities and increased the stability of the nappe flows. The transition flow regime compared reasonably well to the flat and pooled stepped spillways. However, instabilities were observed with a small air-water flow jet at the second pooled weir edge and strong droplet splashing downstream. With increasing discharge, the instabilities disappeared, and the flow became stable in the skimming flow regime (Fig. 3). The larger porosity reduced the transition flow rates and provided a more stable skimming flow regime for smaller flow rates compared with the flat and pooled step configurations. This is also documented in Table 2, listing the changes in flow regimes for the present step configurations and previous data for same channel slope (Felder and Chanson 2011).

On the porous pooled stepped chutes, skimming flow was similar to the observations on the flat and pooled stepped spillways (Fig. 3). Fig. 3 illustrates typical skimming flow patterns for both porous pooled configurations including the air-water flows through the pores. The flow appeared steady, and stable cavity recirculations were observed in the air-water flow region with smaller recirculation motion for the larger porosity. The visual observations suggested a smaller amount of air in the porous pooled step cavities and a smaller interaction between cavity and mainstream flow. The flow through the pores decreased the size of the upward jet at the downstream end of the cavity compared with the pooled steps. Overall the pores affected the air-water cavity flows, but the overlying mainstream flow patterns were close to the corresponding flow regime on the flat and pooled stepped spillways.

It appeared that the porous cavity flow processes were affected by a monophase flow ventilation mechanism. Hence the flows on the porous pooled stepped spillways have similarity with wind flows behind porous fences leading to a reduced recirculation

(a) (b) (c)

Fig. 3. Skimming flow regime on the porous pooled stepped spillways: (a) $d_c/h = 0.99$, $q_w = 0.098$ m^2/s, R $= 3.9 \times 10^5$, $Po = 31\%$; (b) $d_c/h = 1.44$, $q_w = 0.171$ m^2/s, R $= 6.8 \times 10^5$, $Po = 5\%$; (c) $d_c/h = 0.86$, $q_w = 0.079$ m^2/s, R $= 3.1 \times 10^5$, $Po = 31\%$

Table 2. Summary of Changes in Flow Regimes for the Stepped Spillways with Flat, Pooled, and Porous Pooled Steps

Configuration	θ (°)	h (m)	W (m)	w (m)	Po	d_c/h NA-TRA	d_c/h TRA-SK
Flat steps	26.6	0.1	0.52	Not applicable	Not applicable	0.5	0.9
Pooled steps				0.031	0	0.45	0.97
Porous pooled steps				0.031	5%	0.46	0.91
Porous pooled steps				0.031	31%	0.43	0.75
Flat steps (Felder and Chanson 2011)	26.6	0.1	1.0	Not applicable	Not applicable	0.59	0.91
		0.05				0.53	1.06

Note: Comparison with previous data from Felder and Chanson (2011) with same channel slope.

behind the fence with increasing fence porosity (Tsukahara et al. 2012). The injection of fluid into the porous pooled cavity is believed to reduce the overall cavity drag coefficient. The drag reduction behind ventilated bodies was shown by several researchers (e.g., Abdul-Khader and Rai 1980; Suryanarayana et al. 1993; Naudascher and Rockwell 1994). A reduction in drag in the porous pooled stepped experiments would lead to a reduced flow resistance and a reduced energy dissipation performance.

Air-Water Flow Properties

Detailed air-water flow measurements were conducted with a double-tip conductivity probe at all step edges downstream of the inception point for all stepped configurations. The measurements were taken at the step edges for the flat steps ($y = 0$) and at the pool weir edge for the pooled steps ($y = 0$) (Fig. 1). Furthermore, for one skimming flow discharge, detailed measurements were conducted along a pooled step cavity for both the pooled step and the porous pooled step ($Po = 31\%$) configurations.

The void fraction distributions for all stepped configurations showed an S-shape typically observed in previous studies on flat stepped spillways in transition and skimming flows (e.g., Chanson and Toombes 2002; Bung 2011). Little difference was visible between flat, pooled, and porous pooled stepped spillways in a self-similar presentation as function of the dimensionless distance from the (pooled) step edge y/Y_{90} [Fig. 4(a)], where Y_{90} is the distance with void fraction $C = 90\%$. The distributions had an uncertainty of approximately 4% linked with the measurement of the void fraction as well as the characteristic depth, Y_{90}. For all step configurations, the distributions of void fraction matched the advective diffusion self-similar equation for air bubbles in skimming flows reasonably well (Chanson and Toombes 2002)

$$C = 1 - \tanh^2\left[\left(K' - \frac{y/Y_{90}}{2 \times D_o}\right) + \frac{(y/Y_{90} - 1/3)^3}{3 \times D_o}\right] \quad (3)$$

where K' = integration constant; and D_o = function of the mean air concentration C_{mean} only

$$K' = K^* + 1/2 \times D_o - 8/81 \times D_o \quad (4)$$

$$C_{mean} = 0.7622 \times [1.0434 - \exp(-3.614 \times D_o)] \quad (5)$$

K^* = dimensionless constant. The mean air-concentration C_{mean} characterized the depth-averaged air content in terms of Y_{90}

$$C_{mean} = 1 - \frac{\int_{y=0}^{y=Y_{90}} (1 - C) \times dy}{Y_{90}} \quad (6)$$

The derivation of Eq. (3) is briefly outlined in the appendix. In a region closest to the pooled weir edge, small differences between void fraction data and the advective diffusion equation [Eq. (3)] were observed [Fig. 4(a)]. The void fraction measurements had an uncertainty of approximately 2%, and the dimensionless positioning of the probe y/Y_{90} is also affected by uncertainty of approximately 2%, which is mainly linked with the characteristic position, Y_{90}. Overall, the uncertainty of the void fraction measurements is approximately 4%. The agreement between the void fraction data and Eq. (3) was analyzed, and the root mean square errors are added to Fig. 4(a).

A dimensionless void fraction profile based upon the Froude similitude showed also small differences [Fig. 4(b)]. In the Froude similitude, the void fraction is shown as a function of the dimensionless distance from step edge $(y + w)/d_c$. The data showed an upward shift of the void fraction profile for the pooled steps by w/d_c [Fig. 4(b)]. The comparison of the (porous) pooled configurations indicated a good agreement between pooled and porous pooled configuration with $Po = 5\%$. The void fraction distributions for the porous pooled stepped spillway with $Po = 31\%$ were slightly lower and showed small differences in terms of flow depth linked with discharges through the pooled weir pores.

The distributions of bubble count rates showed typical shapes with maxima in the intermediate flow region for void fractions between $C = 0.4$ to 0.5 for all step configurations. For all data sets, the number of entrained air bubbles was larger for the flat stepped spillway compared with the (porous) pooled step configurations [Fig. 5(a)]. In Fig. 5(a), typical dimensionless distributions of the bubble count rate $F \times d_c/V_c$ are shown as functions of $(y + w)/d_c$, where V_c is the critical velocity. A close agreement in bubble count rate distributions was observed for the pooled and porous pooled steps with $Po = 5\%$ for all discharges and at all step edges. In contrast, a smaller number of entrained air bubbles was observed for

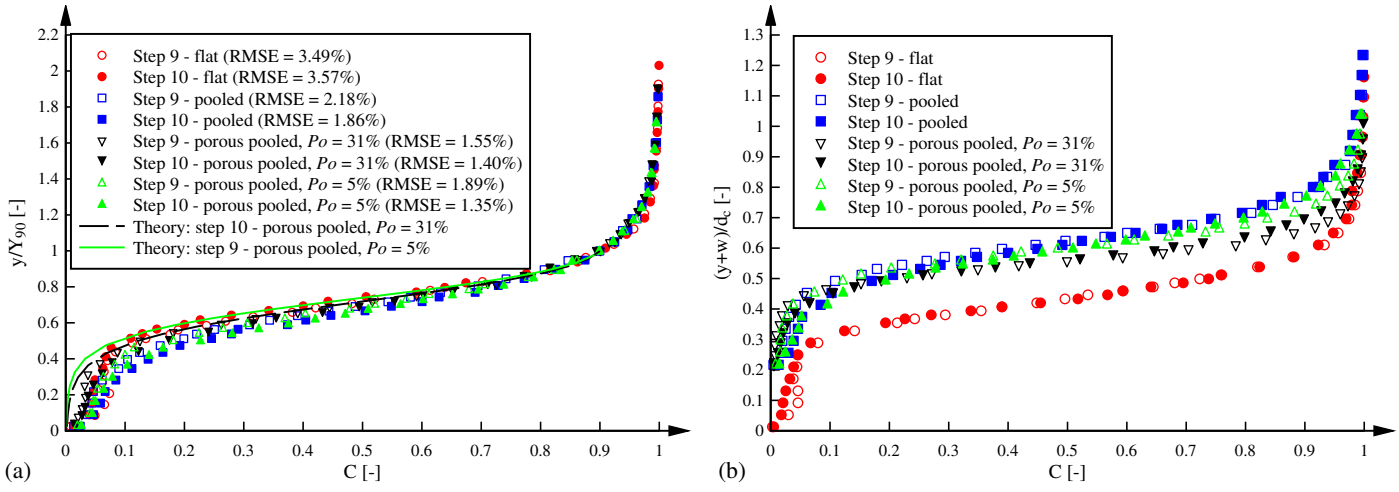

Fig. 4. Void fraction distributions on the stepped spillways with flat, pooled, and porous pooled steps: (a) $d_c/h = 1.29$, $q_w = 0.144$ m^2/s, $R = 5.7 \times 10^5$; comparison with advective diffusion equation [Eq. (3)]; RMSE between experimental data and Eq. (3) added to legend; (b) $d_c/h = 1.52$, $q_w = 0.187$ m^2/s, $R = 7.4 \times 10^5$

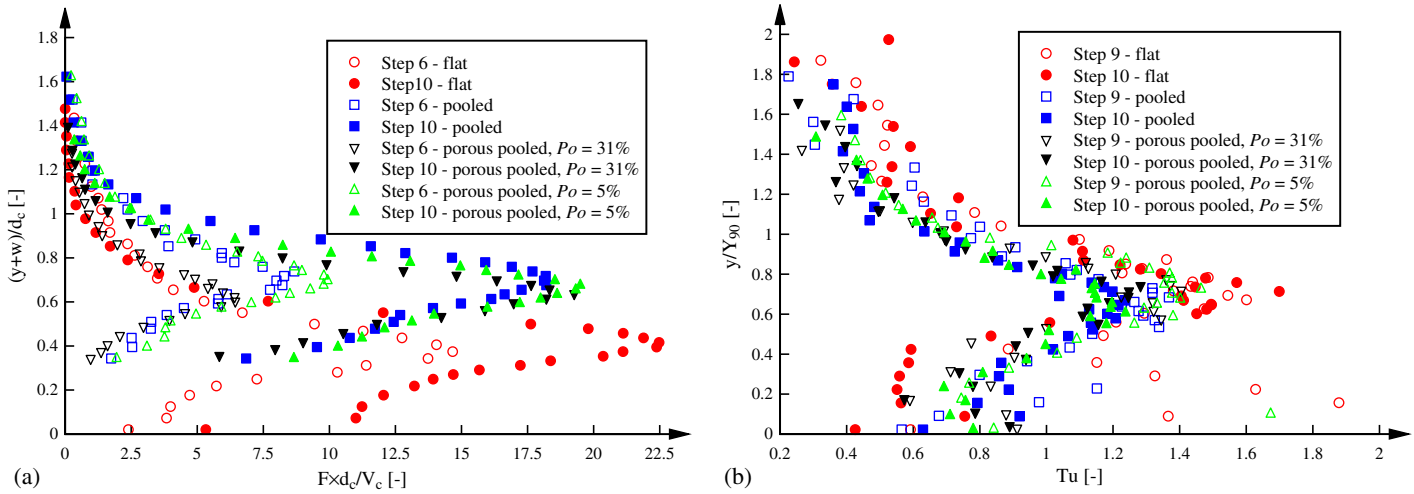

Fig. 5. Bubble count rate and turbulence intensity distributions on the stepped spillways with flat, pooled and porous pooled steps: (a) bubble count rate: $d_c/h = 0.96$, $q_w = 0.094$ m^2/s, R $= 3.7 \times 10^5$; (b) turbulence intensity: $d_c/h = 1.52$, $q_w = 0.187$ m^2/s, R $= 7.4 \times 10^5$

the porous pooled stepped spillway with $Po = 31\%$. The differences in bubble count rate between the configurations tended to decrease with increasing distance from the inception point of air entrainment.

The distributions of turbulence intensity Tu showed little differences qualitatively and quantitatively for the flat, pooled, and porous pooled stepped spillways [Fig. 5(b)]. For all step configurations, maximum turbulence levels were observed in the intermediate flow region, and the values of Tu tended towards small values in the bubbly and spray regions. Slightly larger maximum turbulence levels were observed for the flat stepped spillways in skimming flows [Fig. 5(b)]. Local maxima were found for some step edges in a region close to the step face, which was linked with irregular impingements of air-water flow on the step face. Overall, the turbulence levels were not affected by the introduction of pool weir porosity. Similar results were found in terms of the auto- and cross-correlation time scales, which are characteristic sizes of the transverse and longitudinal air-water vortices. The results can be found in Felder (2013).

The interfacial velocity was calculated based upon the cross-correlation analysis of the air-water raw data of the two conductivity probe tips. For all configurations, the interfacial velocities increased with increasing distance downstream from the inception point. The self-similar presentation of all dimensionless velocity data V/V_{90} for the flat, pooled, and porous pooled stepped spillways were in good agreement [Fig. 6(a)] with V_{90} the interfacial velocity, where $C = 90\%$. The dimensionless velocity V/V_{90} compared very well with a power law with an exponent $1/N = 1/10$ [Fig. 6(a)]

$$\frac{V}{V_{90}} = \left(\frac{y}{Y_{90}}\right)^{1/N} \qquad y/Y_{90} \le 1 \tag{7}$$

The exact value of N may vary from one step edge to the next one for a given flow rate. For $y/Y_{90} > 1$, the velocity distributions had a uniform profile and scatter of the data was observed in the spray region

$$\frac{V}{V_{90}} = 1 \qquad y/Y_{90} > 1 \tag{8}$$

The correlation factor between experimental data and the power law fit is added to the legend in Fig. 6(a) to highlight the close agreement.

Differences between the stepped configurations were observed in terms of the dimensionless interfacial velocities V/V_c in the Froude similitude illustrated as a function of $(y + w)/d_c$ [Fig. 6(b)]. For all present experiments, the data implied smaller interfacial velocities on the flat stepped spillway. This finding was counterintuitive because it was assumed that the pooled steps increased the chute roughness and would slow down the spillway flows. However, the comparison of the equivalent clear water flow depth between the flat and pooled stepped spillways showed consistently a smaller flow depth for the pooled stepped design and hence a faster flow motion down the pooled stepped chutes ($\theta = 26.6°$).

The comparison between interfacial velocities on the pooled and porous pooled stepped spillways was less definite. The interfacial velocities of all pooled and porous pooled designs were in relatively close agreement close to the pool weir edge for $(y + w)/d_c < 0.6$ with almost identical distributions for the pooled steps and the porous pooled design with $Po = 5\%$. However, the free-stream velocities suggested a slightly smaller velocity for the porous pooled stepped design with $Po = 5\%$ and a close agreement for the pooled stepped spillway velocity with more porous pooled steps ($Po = 31\%$) [Fig. 6(b)]. The differences in interfacial velocities could not be directly related accurately to differences in flow depth because the exact contribution of the pores to the flow discharge was unknown. It is believed that the pores affected the flow processes in the step cavity, including a drag reduction in a manner similar to fluid injection in monophase separated flows (Wood 1964; Naudascher and Rockwell 1994). This is associated with a decrease of the cavity recirculations and of the exchange processes between cavity and mainstream flow. Fig. 6(c) illustrates the interfacial velocity distributions at several positions along the step cavity for the pooled step design and the porous pooled configuration with $Po = 31\%$. Some velocity data are also shown within the pooled cavity highlighting the velocity immediately behind the porous wall, showing a uniform distribution of the interfacial velocities. At the same measurement position, the velocities for the pooled stepped configuration showed negative velocities, highlighting the recirculation motions within the step cavity [Fig. 6(c)]. Furthermore, the porous pooled step velocity data were slightly larger in the region above the pseudobottom, whereas the pooled step velocity was slightly larger in the free-stream. Fig. 6(c) highlights the effects of the porous flow upon the step cavity processes and the interfacial velocities in the different flow regions. Further, that

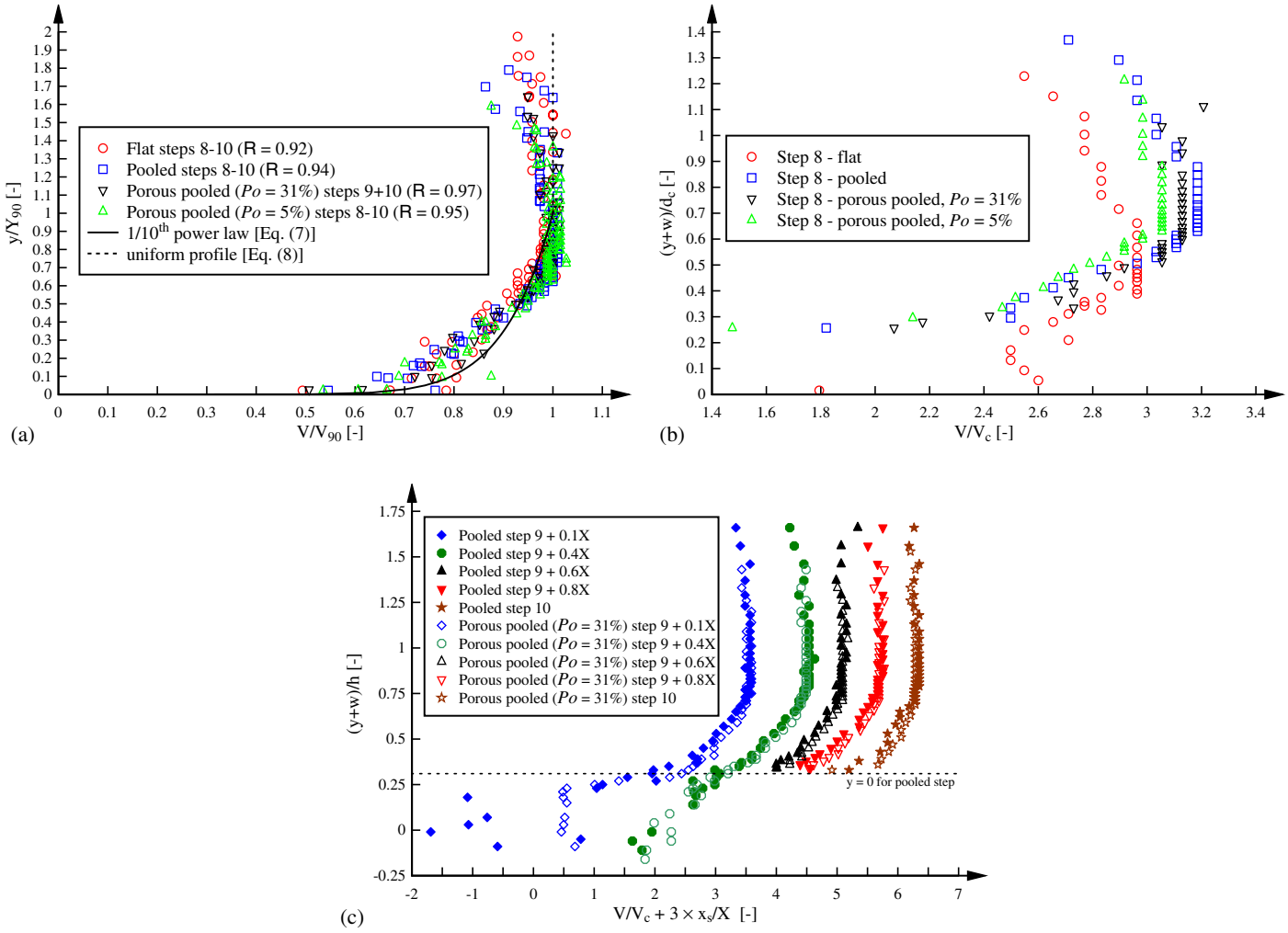

Fig. 6. Interfacial velocity distributions on the stepped spillways with flat, pooled, and porous pooled steps: (a) $d_c/h = 1.52$, $q_w = 0.187$ m^2/s, R $= 7.4 \times 10^5$; comparison with Eqs. (7) and (8); correlation coefficient between experimental data and Eq. (7) added to legend; (b) $d_c/h = 1.29$, $q_w = 0.144$ m^2/s, R $= 5.7 \times 10^5$; (c) interfacial velocity distributions along pooled step cavity: $d_c/h = 1.29$, $q_w = 0.144$ m^2/s, R $= 5.7 \times 10^5$

the flow depth for the porous pooled configurations varied along the step cavity while it remained steady for the pooled step. It appears that an explanation on the differences in interfacial velocities between pooled and porous pooled stepped spillways may be complex because differences were observed for the different flow regions. Further experiments on porous pooled steps would provide a better idea about the flow processes resulting in smaller interfacial velocities in the free-stream.

For all experimental configurations, the microscopic air-water flow properties were recorded at the (pooled) step edges. Typical probability distribution functions of chord sizes are illustrated in Fig. 7. For both air bubble and water droplet chord size distributions,

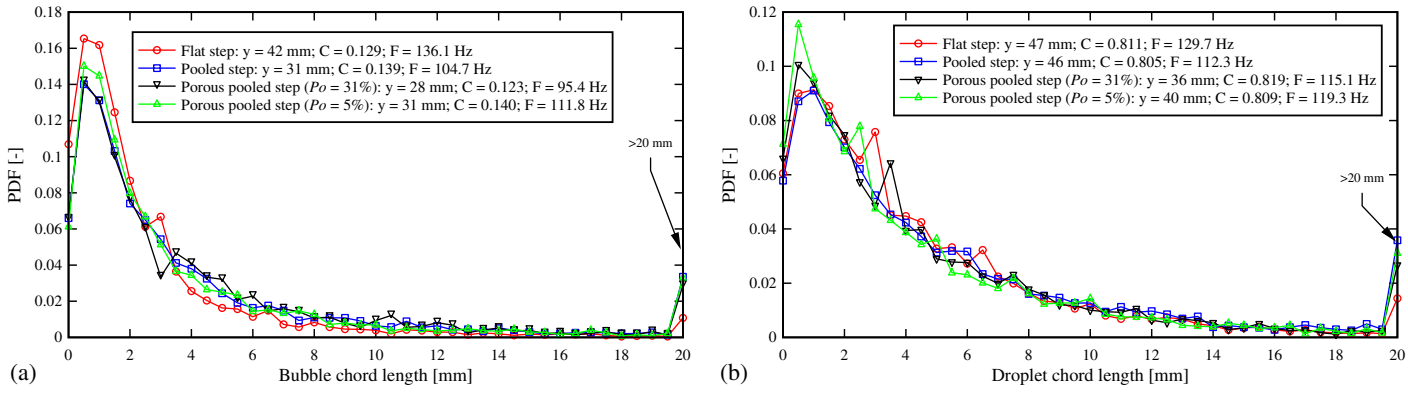

Fig. 7. Chord size PDFs on the stepped spillways with flat, pooled, and porous pooled steps: (a) air bubble chord length: $d_c/h = 1.29$, $q_w = 0.144$ m^2/s, R $= 5.7 \times 10^5$, Step 10; (b) water droplet chord length: $d_c/h = 0.82$, $q_w = 0.073$ m^2/s, R $= 2.9 \times 10^5$, Step 10

a good agreement between the bubble and droplet chord lengths was observed for the flat and (porous) pooled steps. It appeared that the flat stepped spillway showed slightly larger numbers of smaller bubble and droplet chord sizes (Fig. 7).

Energy Dissipation Performance and Flow Resistance

For engineering designs, the energy dissipation rates and the residual energy of stepped spillways are key parameters. The rate of energy dissipation and the residual energy were calculated in this study at the downstream end for all stepped spillway configurations based upon the air-water flow measurements. All stepped spillways dissipated a significant amount of its flow energy compared with the smooth chute design. The residual energy H_{res} at the location of measurement was calculated as follows:

$$H_{res} = \int_0^{Y_{90}} (1-C) \times \cos\theta \times dy + \frac{q_w^2}{2 \times g \times (\int_0^{Y_{90}} (1-C) \times dy)^2} + w \quad (9)$$

The dimensionless residual head H_{res}/d_c at the last step edge or pool weir edge for all discharges is illustrated in Fig. 8 as a function of the dimensionless discharge. Differences in the residual head were observed for the different step configurations with smallest residual energy for the flat steps. On the flat stepped spillway, the residual head decreased with increasing discharge for the smaller flow rates, whereas it was about constant for the largest flow rates. For the pooled and porous pooled steps, the residual energy decreased with increasing flow rates. The largest residual energy was observed for the porous pooled stepped spillways, which was linked with the reduced momentum exchange between cavity and mainstream flow caused by the pores in the pool weir. The pores in the pooled weir reduced both the energetic recirculation motions in the pooled step cavity and the form drag of the steps.

In Fig. 8, the residual head data were compared with previous air-water flow data on flat stepped spillways with the same channel slope and step heights of 5 and 10 cm (Felder and Chanson 2011). The data with $h = 10$ cm were relatively close with the present flat step data for $d_c/h > 1.2$ in the skimming flow regime. However, the smaller step height showed consistently larger residual energy, which was linked with scale effects on the stepped spillway (Felder and Chanson 2009b). Felder and Chanson (2009a) reanalyzed a large amount of experimental data for moderate slope stepped spillways, and the median residual heads are illustrated in Fig. 8 with dashed and dotted lines. The upper dotted line expressed median values for stepped spillway slopes smaller than 15.9°, and the lower dashed line the median values for flat stepped spillway data with slopes $21.8° < \theta < 26.6°$ (Felder and Chanson 2009a). The present flat step data agreed reasonable well with the median values, whereas the (porous) pooled stepped configurations showed larger residual energy (Fig. 8).

On stepped spillways, significant form losses are caused by the steps (Chanson 2001). Additional flow resistance might be caused by the weir on pooled stepped spillways. The flow resistance is commonly expressed by the Darcy-Weisbach friction factor, f_e (Rajaratnam 1990; Chanson 2001). The friction factor on a stepped spillway is the average shear stress between the skimming flow and the cavity regions. In the present study, no uniform equilibrium flow was achieved along the stepped chutes. The Darcy friction factor was deduced from the friction slope (Chanson et al. 2002) as follows:

$$f_e = \frac{8 \times g \times S_f \times (\int_0^{Y_{90}} (1-C) \times dy)^3}{q_w^2} \quad (10)$$

where the friction slope equals $S_f = -\partial H/\partial x$; and x = distance in flow direction (Henderson 1966; Chanson 2001). The experimental results for all stepped spillway configurations are summarized in Fig. 9, in which the friction factor is plotted as a function of the dimensionless step cavity height k_s/D_H in which D_H is the hydraulic diameter. Fig. 9 includes both transition and skimming flow data. The data were compared with the solution of a simplified analytical mixing length model (Chanson 2001; Chanson et al. 2002), which expressed the pseudoboundary shear stress

$$f_d = \frac{2}{\sqrt{\pi} \times K} \quad (11)$$

where f_d = equivalent Darcy friction factor estimate of the form drag; and $1/K$ = dimensionless rate of expansion of the shear layer with $K = 6$ for a velocity between 2 and 6 m/s (Brattberg et al. 1998).

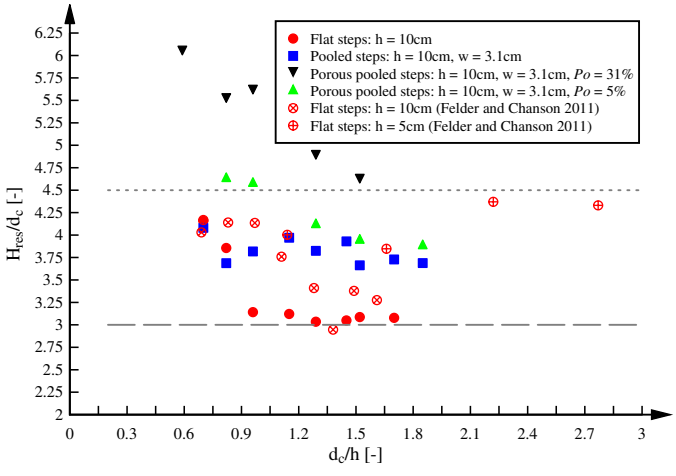

Fig. 8. Dimensionless residual head at the downstream end on the stepped spillways with flat, pooled, and porous pooled steps; comparison with correlations of further stepped spillways with embankment dam slopes (dashed and dotted lines) and data from Felder and Chanson (2011) with same channel slope

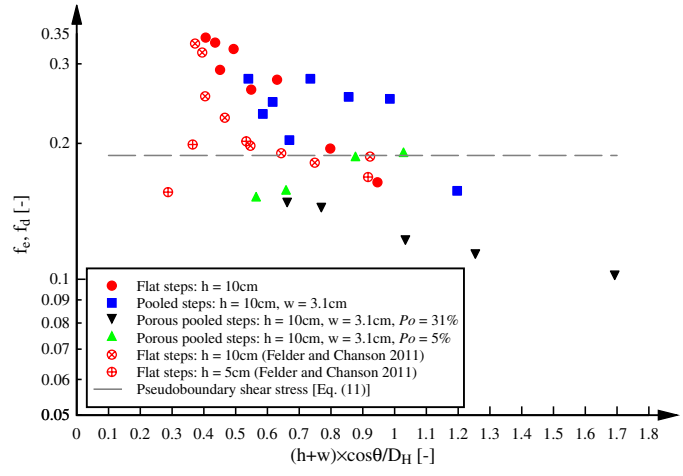

Fig. 9. Darcy friction factors on the stepped spillways with flat, pooled, and porous pooled steps; comparison with pseudoboundary shear stress [Eq. (11)] and previous data from Felder and Chanson (2011) with same channel slope

Overall, the stepped spillway configurations had Darcy-Weisbach friction factors between 0.1 and 0.34 (Fig. 9). The present findings were consistent with the reanalyses of flow resistance data showing variations of Darcy friction factors between 0.1 and 0.35 for $\theta = 15.9°$ and $\theta = 21.8°$ (Felder and Chanson 2009a). For the present configurations, the smallest values of f_e were observed for the porous pooled steps, which confirmed the reduction of form drag and momentum exchange by the pores.

Conclusion

Experiments were conducted on several stepped spillway configurations ($\theta = 26.6°$) comprising flat, pooled ($Po = 5$), and porous pooled steps ($Po = 5\%$ and 31%). The comparative study of the stepped designs included the observations of the flow patterns, the macro- and microscopic air-water flow properties, and the energy dissipation performances. The study of porous pooled steps was limited to one pore size, one channel slope, and one step height; and further configurations should be investigated to identify scale effects linked with the pore diameter. The present study was conducted for Reynolds numbers large enough to minimize air-water scale effects.

The flow patterns in nappe, transition, and skimming flows were in relatively close agreement for all configurations. Small instabilities were observed for the pooled stepped spillway in nappe flows, which was linked with pulsating flows in the first pool and instabilities of the free-falling nappes. The introduction of porosity ($Po > 0$) to the pooled weir wall eliminated any flow pulsations, and the flow patterns were stable for all flow discharges. The pores contributed to the discharge and decreased the cavity recirculation and air entrainment into the step cavities. In terms of flow stability, the porous pooled step design was preferable to the pooled stepped design.

The comparison of the air-water flow properties for the flat, pooled, and porous pooled stepped spillways was conducted for transition and skimming flows based upon self-similar considerations and qualitative representation in a Froude similitude. The self-similar comparative analyses showed a good agreement in most air-water flow property distributions, including the void fraction, bubble count rate, turbulence levels, and dimensionless interfacial velocity, V/V_{90}. For all flow rates, the comparison highlighted larger interfacial velocities, V/V_c, for the pooled and porous pooled stepped spillways compared with the flat stepped chute, which was linked with a reduction in flow depth. The comparison of the porous pooled steps and the corresponding pooled step was less definite, and the interfacial velocities differed in the different regions of the flow. The detailed investigation of the pooled cavity flows behind the porous pooled wall highlighted the pore discharge and the change in cavity recirculation.

The comparison of the residual energy at the downstream end showed a smaller energy dissipation rate for the pooled and porous pooled stepped spillways. The larger residual energy on the pooled stepped spillway was associated with an increased flow velocity and a smaller flow depth compared with the flat design. The porous pooled steps induced a reduction in form drag in the cavities, thus decreasing the momentum exchange between cavity recirculation and main stream flow. Hence, the porous pooled steps exhibited smaller energy dissipation performance and smaller friction factors. The porous pooled stepped design is therefore disadvantageous compared with the flat step design, which appeared to be the preferred design option in terms of flow stability and energy dissipation rate.

Appendix. Advective Diffusion Equation of Air Bubbles

Wood (1984) and Chanson (1997) developed an analytical model to predict the advective diffusion of air bubbles in air-water free-surface flows. The analytical equation is based upon the hypothesis of uniform equilibrium conditions, i.e., the air concentration is constant in the flow direction. This assumption is not entirely correct because experimental data highlight a rapid aeration just downstream of the inception point of free-surface aeration before equilibrium air concentration is reached further downstream. A further characteristic air-water flow parameter, the number of entrained air bubbles, appears to not reach uniform equilibrium flow conditions.

Despite these limitations, equilibrium conditions were assumed for the integration of the continuity equation for the air content (Chanson 1997)

$$\frac{\partial C}{\partial y'} = \frac{1}{D'} \times C \times \sqrt{1 - C} \tag{12}$$

where $y' = y/Y_{90}$; and $D' = D_t/u_r \times \cos\theta \times Y_{90})$ denotes a dimensionless turbulent diffusivity in which D_t is the turbulent diffusivity; u_r = bubble rise velocity; θ = channel slope; and y = distance perpendicular to the mean flow direction. D' is the ratio of the air bubble diffusion coefficient to the rise velocity component normal to the flow direction times the characteristic transverse dimension of the shear flow. Chanson and Toombes (2002) expressed the dimensionless bubble diffusivity D' as

$$D' = \frac{D_o}{1 - 2 \times (\frac{y}{Y_{90}} - \frac{1}{3})^2} \tag{13}$$

and Eq. (12) becomes

$$C = 1 - \tanh^2\left[\left(K' - \frac{y/Y_{90}}{2 \times D_o}\right) + \frac{(y/Y_{90} - 1/3)^3}{3 \times D_o}\right] \tag{14}$$

where tanh = hyperbolic tangent function; K' and D_o = functions of the mean void fraction C_{mean} only; and Y_{90} is the characteristic distance in which $C = 0.90$. Hence, Eq. (14) is valid within the boundaries $0 \le C \le 0.90$.

The advective diffusion equation [Eq. (14)] has been applied in many studies of air-water free-surface flows with various channel slopes and step configurations. Although the concept of uniform equilibrium flow conditions on stepped spillways might not be achieved, experimental results highlighted the successful application of the advective diffusion equation in gradually varied flows (e.g., Matos 2000; Gonzalez and Chanson 2008; Bung 2011; Felder 2013).

Acknowledgments

The authors thank Jason Van Der Gevel and Stewart Matthews for their technical assistance. The financial supports through a UQ research scholarship and through the Australian Research Council (Grant DP120100481) are acknowledged.

Notation

The following symbols are used in this paper:

C = void fraction or air content;
C_{mean} = mean air concentration;
D' = dimensionless turbulent diffusivity;
D_t = turbulent diffusivity;

D_H = hydraulic diameter (m);
D_o = dimensionless constant of the depth-averaged air concentration;
d_c = critical flow depth (m);
F = bubble count rate (Hz);
f_d = Darcy friction factor estimated from form drag;
f_e = equivalent Darcy friction factor;
g = gravity acceleration constant (m/s^2);
H = total head (m);
H_{res} = residual energy (m);
h = step height (m);
K = expansion rate of shear layer;
K' = dimensionless constant function of the depth-averaged air concentration;
k_s = step cavity height (m);
l_w = pool weir length (m);
N = exponent;
Po = porosity of porous pooled steps;
q_w = water discharge per unit width (m^2/s);
S_f = friction slope;
Tu = turbulence intensity;
U_{Po} = flow velocity through pores (m/s);
u_r = bubble rise velocity (m/s);
V = interfacial velocity (m/s);
V_c = critical flow velocity (m/s);
V_{90} = interfacial velocity where $C = 90\%$ (m/s);
W = channel width (m);
w = pool weir height (m);
X = length of step cavity (m);
x = flow direction;
x_s = distance along a single step cavity (m);
Y_{90} = characteristic flow depth, where $C = 90\%$ (m);
y = direction normal to the pseudobottom formed by the step edges;
Ø = diameter of pores and probe tips (m);
$\Delta H_{(Po)}$ = piezometric head difference between the two sides of the porous wall (m);
Δx = longitudinal separation between probe tips (m);
Δz = transverse separation between probe tips (m);
ζ = resistance coefficient; and
θ = channel slope.

References

Abdul-Khader, M. H., and Rai, S. P. (1980). "A study of channel obstructions with a longitudinal slot." *Proc., 7th Australasian Hydraulics and Fluid Mechanics Conf., IEAust.*, Brisbane, Australia, 175–178.

André, S. (2004). "High velocity aerated flows on stepped chutes with macro-roughness elements." Ph.D. thesis, Laboratoire de Constructions Hydraulics (LCH), EPFL, Lausanne, Switzerland, 272.

Baker, R. (1994). "Brushes clough wedge block spillway-progress report no. 3." *SCEL Project Rep. No. SJ542-4*, Univ. of Salford, U.K., 47.

Boes, R., and Hager, W. (2003). "Two-phase flow characteristics of stepped spillways." *J. Hydraul. Eng.*, 10.1061/(ASCE)0733-9429(2003)129:9(661), 661–670.

Brattberg, T., Chanson, H., and Toombes, L. (1998). "Experimental investigations of free-surface aeration in the developing flow of two-dimensional water jets." *J. Fluids Eng.*, 120(4), 738–744.

Bung, D. B. (2011). "Developing flow in skimming flow regime on embankment stepped spillways." *J. Hydraul. Res.*, 49(5), 639–648.

Chamani, M., and Rajaratnam, N. (1999). "Characteristics of skimming flow over stepped spillways." *J. Hydraul. Eng.*, 10.1061/(ASCE)0733-9429(1999)125:4(361), 361–368.

Chanson, H. (1994). "Hydraulics of skimming flows over stepped channels and spillways." *J. Hydraul. Res.*, 32(3), 445–460.

Chanson, H. (1997). *Air bubble entrainment in free-surface turbulent shear flows*, Academic, London, 401.

Chanson, H. (2001). *The hydraulics of stepped chutes and spillways*, Balkema, Lisse, The Netherlands, 418.

Chanson, H., and Toombes, L. (2002). "Air-water flows down stepped chutes: Turbulence and flow structure observations." *Int. J. Multiphase Flow*, 28(11), 1737–1761.

Chanson, H., Yasuda, Y., and Ohtsu, I. (2002). "Flow resistance in skimming flows and its modelling." *Can. J. Civ. Eng.*, 29(6), 809–819.

Felder, S. (2013). "Air-water flow properties on stepped spillways for embankment dams: Aeration, energy dissipation and turbulence on uniform, non-uniform and pooled stepped chutes." Ph.D. thesis, Univ. of Queensland, Australia.

Felder, S., and Chanson, H. (2009 a). "Energy dissipation, flow resistance and gas-liquid interfacial area in skimming flows on moderate-slope stepped spillways." *Environ. Fluid Mech.*, 9(4), 427–441.

Felder, S., and Chanson, H. (2009b). "Turbulence, dynamic similarity and scale effects in high-velocity free-surface flows above a stepped chute." *Exp. Fluids*, 47(1), 1–18.

Felder, S., and Chanson, H. (2011). "Energy dissipation down a stepped spillway with nonuniform step heights." *J. Hydraul. Eng.*, 10.1061/(ASCE)HY.1943-7900.0000455, 1543–1548.

Felder, S., and Chanson, H. (2012). "Free-surface profiles, velocity and pressure distributions on a broad-crested weir: A physical study." *J. Irrig. Drain. Eng.*, 10.1061/(ASCE)IR.1943-4774.0000515, 1068–1074.

Felder, S., and Chanson, H. (2013a). "Aeration, flow instabilities, and residual energy on pool stepped spillways of embankment dams." *J. Irrig. Drain. Eng.*, 10.1061/(ASCE)IR.1943-4774.0000627, 880–887.

Felder, S., and Chanson, H. (2013b). "Air-water flow measurements in a flat slope pooled stepped waterway." *Can. J. Civ. Eng.*, 40(4), 361–372.

Gonzalez, C. A., and Chanson, H. (2007). "Hydraulic design of stepped spillways and downstream energy dissipators for embankment dams." *Dam Eng.*, 17(4), 223–244.

Gonzalez, C. A., and Chanson, H. (2008). "Turbulence and cavity recirculation in air-water skimming flows on a stepped spillway." *J. Hydraul. Res.*, 46(1), 65–72.

Guenther, P., Felder, S., and Chanson, H. (2013). "Flow aeration, cavity processes and energy dissipation on flat and pooled stepped spillways for embankments." *Environ. Fluid Mech.*, 13(5), 503–525.

Henderson, F. M. (1966). *Open channel flow*, MacMillan, New York, 522.

Idelchik, I. E. (1994). *Handbook of hydraulic resistance*, 3rd Ed., CRC, Boca Raton, 790.

Kökpinar, M. A. (2004). "Flow over a stepped chute with and without macro-roughness elements." *Can. J. Civ. Eng.*, 31(5), 880–891.

Matos, J. (2000). "Hydraulic design of stepped spillways over RCC dams." *Int. Workshop on Hydraulics of Stepped Spillways*, H. E. Minor and W. H. Hager, eds., Balkema, Zürich, Switzerland, 187–194.

Naudascher, E., and Rockwell, D. (1994). *Flow-induced vibrations. An engineering guide. IAHR hydraulic structures design manual No. 7, hydraulic design considerations*, Balkema, Rotterdam, Netherlands, 413.

Ohtsu, I., Yasuda, Y., and Takahashi, M. (2004). "Flow characteristics of skimming flows in stepped channels." *J. Hydraul. Eng.*, 10.1061/(ASCE)0733-9429(2004)130:9(860), 860–869.

Peyras, L., Royet, P., and Degouette, G. (1992). "Flow and energy dissipation over stepped gabion weirs." *J. Hydraul. Eng.*, 10.1061/(ASCE)0733-9429(1992)118:5(707), 707–717.

Rajaratnam, N. (1990). "Skimming flow in stepped spillways." *J. Hydraul. Eng.*, 10.1061/(ASCE)0733-9429(1990)116:4(587), 587–591.

Relvas, T. R., and Pinheiro, A. N. (2008). "Inception point and air concentration in flows on stepped chutes lined with wedge-shaped concrete blocks." *J. Hydraul. Eng.*, 10.1061/(ASCE)0733-9429(2008)134:8(1042), 1042–1051.

Suryanarayana, G. K., Pauer, H., and Meier, G. E. A. (1993). "Bluff-body drag reduction by passive ventilation." *Exp. Fluids*, 16(2), 73–81.

Thorwarth, J. (2008). "Hydraulisches Verhalten der Treppengerinne mit eingetieften Stufen—Selbstinduzierte Abflussinstationaritäten und Energiedissipation [Hydraulics of pooled stepped spillways—Self-induced

unsteady flow and energy dissipation].” Ph.D. thesis, Univ. of Aachen, Germany (in German).
Toombes, L. (2002). “Experimental study of air-water flow properties on low-gradient stepped cascades.” Ph.D. thesis, Dept. of Civil Engineering, Univ. of Queensland, Australia.
Tsukahara, T., Sakamoto, Y., Aoshima, D., Yamamoto, M., and Kawaguchi, Y. (2012). “Visualisation and laser measurements on the flow field and sand movement on sand dunes with porous fences.” *Exp. Fluids*, 52(4), 877–890.
Wood, C. J. (1964). “The effect of base bleed on a periodic wake.” *J. Roy. Aeronaut. Soc.*, 68, 477–482.
Wood, I. R. (1984). “Air entrainment in high speed flows.” *Proc., Int. Symp. on Scale Effects in Modelling Hydraulic Structures*, International Association of Hydraulic Research, Esslingen, Germany.